Smart Structures and Systems, *Vol. 26, No. 5* (*2020*) *605-617*
DOI: https://doi.org/10.12989/sss.2020.26.5.605

Numerical simulation of compressive to tensile load conversion for determining the tensile strength of ultra-high performance concrete

Hadi Haeri[1], Nader Mirshekari[2], Vahab Sarfarazi[*3] and Mohammad Fatehi Marji[4]

[1]*State Key Laboratory for Deep GeoMechanics and Underground Engineering, Beijing, 100083, China*
[2]*Department of Civil Engineering, Islamic Azad University, Vramin-Pishva branch, Pishva, Iran*
[3]*Department of Mining Engineering, Hamedan University of Technology, Hamedan, Iran*
[4]*Department of Mine Exploitation Engineering, Faculty of Mining and metallurgy, Institute of Engineering, Yazd University, Yazd, Iran*

(*Received December 29, 2019, Revised April 11, 2020, Accepted June 30, 2020*)

Abstract. In this study, the experimental tests for the direct tensile strength measurement of Ultra-High Performance Concrete (UHPC) were numerically modeled by using the discrete element method (circle type element) and Finite Element Method (FEM). The experimental tests used for the laboratory tensile strength measurement is the Compressive-to-Tensile Load Conversion (CTLC) device. In this paper, the failure process including the cracks initiation, propagation and coalescence studied and then the direct tensile strength of the UHPC specimens measured by the novel apparatus i.e., CTLC device. For this purpose, the UHPC member (each containing a central hole) prepared, and situated in the CTLC device which in turn placed in the universal testing machine. The direct tensile strength of the member is measured due to the direct tensile stress which is applied to this specimen by the CTLC device. This novel device transferring the applied compressive load to that of the tensile during the testing process. The UHPC beam specimen of size 150 × 60 × 190 mm and internal hole of 75 × 60 mm was used in this study. The rate of the applied compressive load to CTLC device through the universal testing machine was 0.02 MPa/s. The direct tensile strength of UHPC was found using a new formula based on the present analyses. The numerical simulation given in this study gives the tensile strength and failure behavior of the UHPC very close to those obtained experimentally by the CTLC device implemented in the universal testing machine. The percent variation between experimental results and numerical results was found as nearly 2%. PFC2D simulations of the direct tensile strength measuring specimen and ABAQUS simulation of the tested CTLC specimens both demonstrate the validity and capability of the proposed testing procedure for the direct tensile strength measurement of UHPC specimens.

Keywords: ultra-high performance concrete; direct tensile strength; compressive to tensile load conversion; finite element method; discrete element method

1. Introduction

The design and safe operation of many geo-engineering structures mainly relies on the tensile strength of brittle materials such as rock and concrete which are weak under tensile loading conditions. Tensile strength determination is generally accomplished through some sophisticated laboratory test setups including direct and indirect experiments. For many years, due to some difficulties associated with direct tests, the indirect tensile strength tests were standardized and used. Because of easy preparation of rock/concrete specimens and their setup simplicity, the Brazilian tensile strength tests are widely used for determining the split tensile strength (Bieniawski and Hawkes 1978, Zhang 2002, Ramadoss and Nagamani 2013, Pan *et al*. 2014, Martin 2014, Shuraim *et al*. 2016, Mohammad 2016, Shaowei *et al.* 2016, Yaylac 2016, Akbas 2016, Liu *et al*. 2018, Shang *et al*. 2018, Liao *et al.* 2019, Aliabadian *et al.* 2019). The double punch tests and the flexural tests on beams (three points and four points bending tests) have also used in the laboratory to experimentally determine the tensile strength of rock and concrete (Zhou 1988, Swaddiwudhipong *et al*. 2003, Chen and Trumbauer 1972, Khan 2012, Kim and Taha 2014, Zain *et al.* 2002, Sardemir 2016, Sarfarazi *et al*. 2017). However, the indirect tensile strength results such as those of Brazilian tests are somewhat overestimated (usually more than 26 percent in most cases) and may produce some problems in the modern applications of geo-mechanics (Gorski *et al*. 2007). Therefore, the direct tensile strength measurements found some new places in the modern geo-mechanic's application because they are able to accurately measure the tensile strength of concrete and rock (Zhou 1988, Wang *et al*. 2004, Ghaffar *et al.* 2005, Erarslan and Williams 2012, Wei and Chau 2013, Kim and Taha 2014, Silva *et al.* 2015, Abrishambaf *et al*. 2015, Sardemir 2016, Wang *et al*. 2004, Zhang *et al*. 2016, Alhussainy *et al*. 2016, Sarfarazi *et al.* 2016, Omar *et al.* 2018, Quang *et al*. 2019). The direct tensile strength of concrete can be determined by performing some special direct pull tests on dumb-bell shaped rock like specimens which are specifically designed and prepared in a rock mechanics laboratory (Xie and Liu 1989, Zheng *et al*. 2001, Sardemir 2016, ASTM D2936-08

*Corresponding author, Associate Professor,
E-mail: vahab.sarfarazi@gmail.com

ISSN: 1738-1584 (Print), 1738-1991 (Online)

Table 1 The concrete material definition in finite element analyses

Parameter	Value
Dilation angle	56
Eccentricity	0.1
The ratio of initial equibiaxial compressive yields stress to initial uniaxial compressive yield stress	1.16
The ratio of the second stress invariant on the tensile meridian	0.667
Viscosity parameter	0.0001

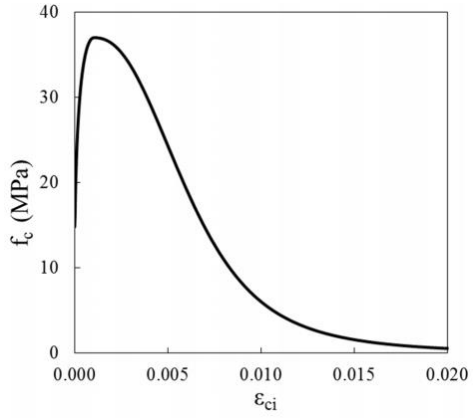

Fig. 1 The stress-strain relationship of concrete

2008).

The mechanical properties of the rock and concrete such as their rapture modulus can be measured by measuring the indirect tensile strengths with 3- and/or 4-point bending tests in which overestimating the real values of the modulus because of the above-mentioned drawbacks in estimating the indirect tensile strength of rock materials (Gorski *et al*. 2007, Ramadoss and Nagamani 2006, 2008, 2013, Ramadoss 2014). Other numerical methods, such as Peridynamics (PD) (Zhou and Wang 2016), the extended finite element method (Zhou *et al*. 2008) and general particle dynamics (Zhou *et al*. 2015, Bi *et al*. 2016) have been done on the crack propagation.

The present research, tried to suggest a direct tensile testing method based on the concept of transferring the applied compressive load to that of the direct tensile during the testing. The proposed direct tensile testing machine uses a sophisticated Compression-to-Tensile Loading Convertor (CTLC) containing the specimen to be tested. This specimen should be specifically prepared from rock or concrete samples.

2. Finite element simulation using ABAQUS software

The standard finite element code knows as ABAQUS is used in this study to numerically simulate the inelastic behavior of concrete based on the Concrete Damaged Plasticity (CDP) model. ABAQUS is a general purpose computer software used for the analyses of wide range of linear and non-linear elastic problems related to brittle and quasi-brittle materials such as rock and concrete. The tensile and compressive loading conditions in rock and concrete may be modeled by considering the isotropic damaged elasticity concept (Hibbitt *et al*. 2012). Table 1 gives the CDP parameters used in the finite element method (ABAQUS).

The constitutive models for the behavior of concrete under uniaxial compressive and tensile conditions can be used to define the CDP model in ABAQUS. For example, the constitutive equations such as the following stress-strain relations can be used considering both the uniaxial compression and tension, respectively (Hibbitt *et al*. 2012)

$$\sigma_c = (1 - d_c)E_0(\varepsilon_c - \varepsilon_c^{pl}) \quad (1)$$

$$\sigma_t = (1 - d_t)E_0(\varepsilon_t - \varepsilon_t^{pl}) \quad (2)$$

where E_0 is the initial elastic modulus of the material. The plastic strains, ε_c^{pl} and ε_t^{pl} are defined for compression and tension, respectively. d_c and d_t are damage variables in compression and tensile test, respectively. These parameters are defined between 0-1 based on the plastic strain. These variables increase by increasing in plastic strain. The variables are equal to zero, when there is not any plastic strain in the model. In this condition, the compressive strength or tensile strength are obtained according to Hoek's Equation (Hibbitt *et al*. 2012).

The pre and post peak uniaxial compressive stresses of concrete are considered and the unconfined concrete model code of CEB-FIB 2010 is used considering the pre-peak strength of the material. In the finite element method, the analysis of concrete's post-peak behavior under tension and compression can be relatively mesh sensitive (Mier 1986, Hillerborg 1989, CEB-FIB 2010). Therefore, in the present analysis, the effect of mesh size is considered by using the post-peak compression models of Vonk (1993) and Van Mier (1992). The CPD model of ABAQUS is used to investigate the compressive behavior of concrete which relates the stress to inelastic strain (i.e., the fc-ε_{ci}). Fig. 1 shows the uniaxial compressive behavior of concrete modeled by FEM in ABAQUS software.

The linear elastic behavior of concrete up to its peak tensile level is considered to obtain the peak tensile modulus which is calculated as the ratio of peak tensile stress to that of its corresponding peak strain of the material. This peak tensile strength (i.e., f_{ctm} in MPa) can be evaluated by using the following equation (CEB-FIB 2010).

$$f_{ctm} = 0.3(f_{ck})^{2/3} \quad (3)$$

The undesirable mesh sensitivity (mentioned above) can be avoided by defining the strain softening behavior in form of the stress vs crack opening displacement graph (f_{ct}-w). The fracture energy (G_f in MPa) required to keep open a unit area of a crack surface is defined based on the brittle fracture concept as shown in Fig. 2(c) (Hibbitt *et al*. 2012). In the computer code of CEB-FIB 2010 model the fracture energy, G_f, can be calculated from the concrete's normal

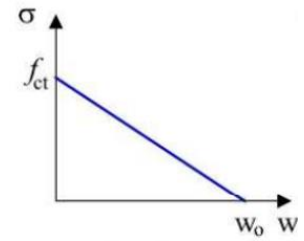

(a)

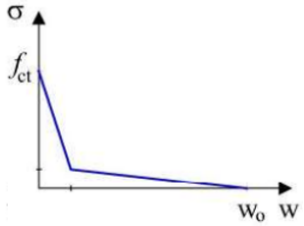

(b)

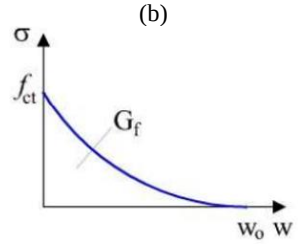

(c)

Fig. 2 Post-peak cracking tensile behavior of concrete
(a) linear; (b) bilinear; (c) exponential

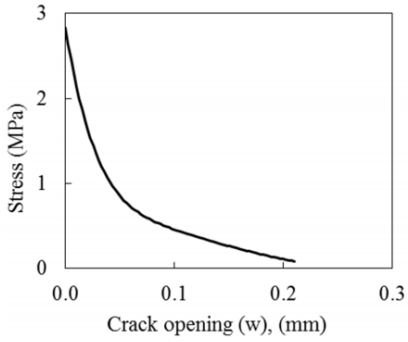

Fig. 3 Stress-crack opening behavior for tension

weight (in the absence of experimental data) as follows

$$G_f = 0.073(f_{cm})^{0.18} \quad (4)$$

$$f_{cm} = f_{ck} + \Delta f \quad (5)$$

where f_{cm} is the mean compressive strength (MPa). Δf is a constant which and is taken as 8 MPa in this study. G_f is calculated from Eq. (4) because there was no experimental data for this parameter in the literature. However, there are three different types of models explaining the tensile softening behavior of the cracked specimens known as linear, bilinear and exponential models. Fig. 2 shows the corresponding stress-crack opening displacement (COD) curve for this model.

However, in this research, the tensile softening behavior of concrete is considered to be measured after the cracking portion of the post-peak stress. Fig. 3 shows the stress-COD curve representing the exponential form of post-peak tensile softening model of Hordijk (1992). In the ABAQUS software, the lower limit of the post-cracking stress which equals to one hundredth of the initial cracking stress (i.e., $\sigma \geq f_{ct}/100$) is adopted to avoid the potential numerical problems that may arises during the stability analysis of the concrete specimens (Hibbitt *et al*. 2012). Therefore, the values of post-cracking stress can be well defined in the FEM by taking into account such numerical limitations.

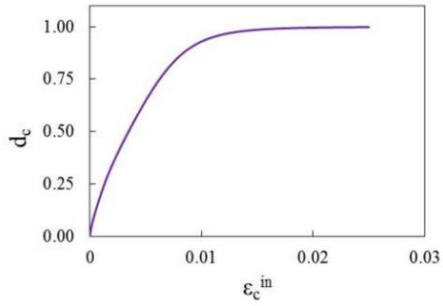

(a)

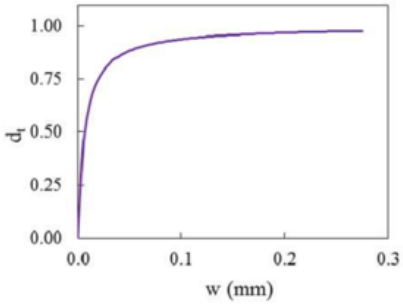

(b)

Fig. 4 Damage behaviors of the concrete
(a) compressive damage; (b) tensile damage

Accordingly, considering the two independent uniaxial compressive, the degraded response process of concrete specimens and the tensile damage variables (i.e., d_c and d_t) all are defined in FEM used for CDP model. In this model, these two variables represent the possible damage that may occur in the concrete specimen due to degradation of elastic stiffness during the unloading process. This phenomenon can be easily visualized in the strain softening portion of the actual stress-strain curves showing the real behavior of the modeled specimens. The elastic stiffness degradation can be considerably different for the cases of compressive and tensile behaviors of concrete. Therefore, it may be concluded that the plastic strain, the temperature and the other field variables all affecting the uniaxial degradation variables of concrete specimens, their tensile and compressive behaviors. These brittle materials corresponding to their damage degrees i.e., ranging from the undamaged to fully damaged materials can be modeled by FEM (Hibbitt *et al*. 2012). Fig. 4 demonstrates the tensile and compressive damage behaviors of the concrete specimens modeled for FEA.

It is usually more difficult to measure the direct tensile strength of concrete specimens in the laboratory. Therefore,

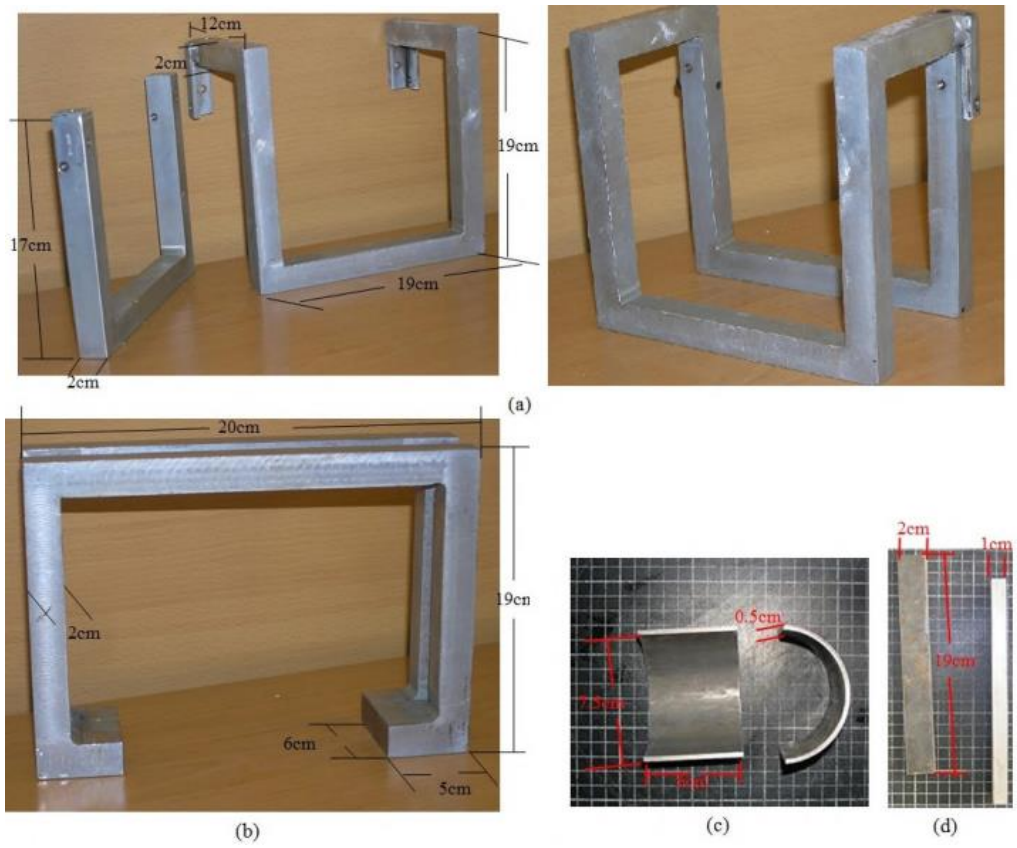

Fig. 5 Different parts of CTLC device

Table 2 The mixture proportions used for batching of the specimens

Gravel (g)	Sand (g)	Cement (g)	Water (cc)	Steel fiber (g)	Super plasticizer (g)	Micro silica (g)
3000	10500	2800	1500	14	120	90

Table 3 Properties of cement and Silica fume

Properties	Cement	Silica fume
Physical properties		
Specific gravity (g/cm^3)	3.15	2.2
Surface area (m^2/kg)	320	20000
Size (micron)	-	0.1
Bulk density (kg/m^3)	-	576
Initial setting time (min)	45	-
Final setting time (min)	375	-
Chemical properties (percentage)		
SiO_2	90-96	20-25
Al_2O_3	0.5-0.8	4-8

the CTLC device is developed and used in recent years. Following sections explain the CTLC device and the numerical simulation of this apparatus and the specially used concrete specimens or CTLC specimens. The two-dimensional discrete element method (i.e., PFC2D which is the 2D particle flow code) and ABAQUS software are used to numerically simulate the CTLC concrete specimens.

3. Experimental program

In this experiment program, CTLC apparatus has been developed and introduced. Also, preparation of the Ultra-High Performance Concrete (UHPC) specimen for CTLC test described and tensile test has been introduced. Laboratory measurement has been described in last section.

3.1 Compressive-to-tensile load convertor (CTLC) apparatus

The CTLC device is specially designed to use some specifically prepared concrete specimens for measuring the direct tensile strength of concrete using the conventional laboratory testing machines. The direct tensile strengths of rocks can also be measured by preparing the specimens with a central hole at their centers so that the applied compressive load to the specimen can be transferred to that of tensile as required by CTLC device placed in the universal testing machine.

The main parts of a CTLC device are illustrated in Figs. 5(a)-(d). The “U” shape part (Part I) of the device consists of the two parts “L” and “1” all built from stainless steel (Fig. 5(a)). Fig. 5(b) shows the second part (Part II) of the

Table 4 Physical properties of sand

Index	Value
Specific gravity (g/cm^3)	2.63
Passing 4.75 mm sieve (%)	100
Maximum dry density (KN/m^3)	15.5
minimum dry density (KN/m^3)	12.3
D10	0.194
Particle size (mm), D50	0.322
D60	0.344

Table 5 Fiber specification

Parameter	Value
Length (mm)	50
Diameter (mm)	1
Aspect ratio	50
Density (g/cm^3)	7.85
Tensile strength (MPa)	1000

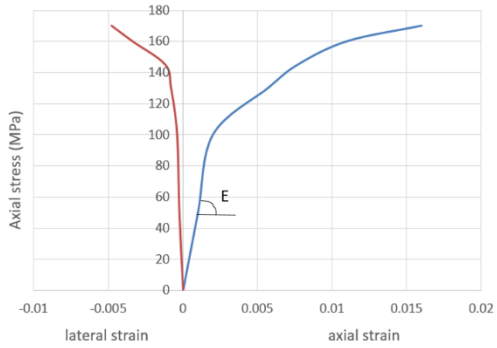

Fig. 6 Axial stress versus axial strain and lateral strain

Table 6 Mechanical properties of concrete

Mechanical properties of concrete	Value
Average uniaxial compressive strength (MPa)	170
Average Young's Modulus in compression (GPa)	55
Average Poisson's ratio	0.19

device with "Π" shape. Part III of the device consists of two stainless sub-segments of semi-cylindrical shape where each segment has the dimensions of 75 mm × 10 mm × 60 mm (Fig. 5(c)). Finally, Fig. 5(d) shows Part VI of the device which consists of two steel blades with 20 mm × 10 mm × 190 mm in dimensions.

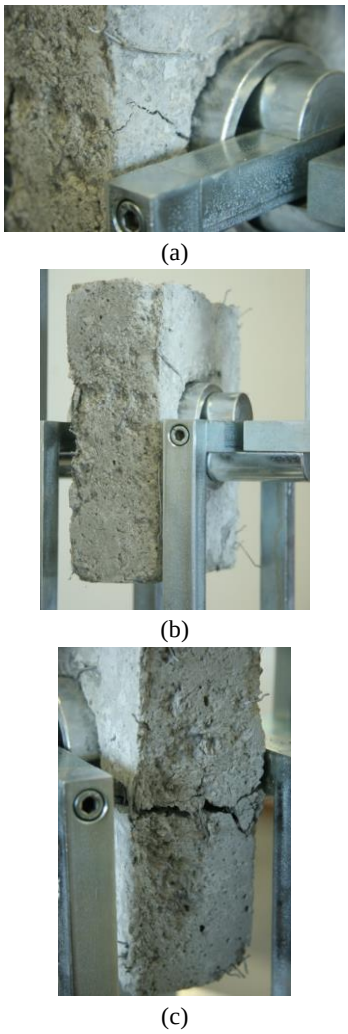

(a)

(b)

(c)

Fig. 7 The set-up procedure of CTLC device

Fig. 8 Universal Tensile Testing Machine (UTTM)

3.1.1 Materials

Concrete specimen was prepared from a mixture of sand, cement, water, steel fiber, super-plasticizer and micro silica. The material proportions used for batching of the specimens are shown in Table 2. Crushed-limestone sand with specific gravity of 2.7 g/cm^3 was used as aggregates. Tables 3-5 shows the properties of materials. The ASTM D29-1986, procedure was followed to conduct the Uniaxial Compressive Strength (UCS) tests. Fig. 6 shows axial stress versus axial strain and lateral strain. Also, the procedure for determination of Young modulus (E) has been depicted in Fig. 6. Table 6 shows the results of the uniaxial compressive test.

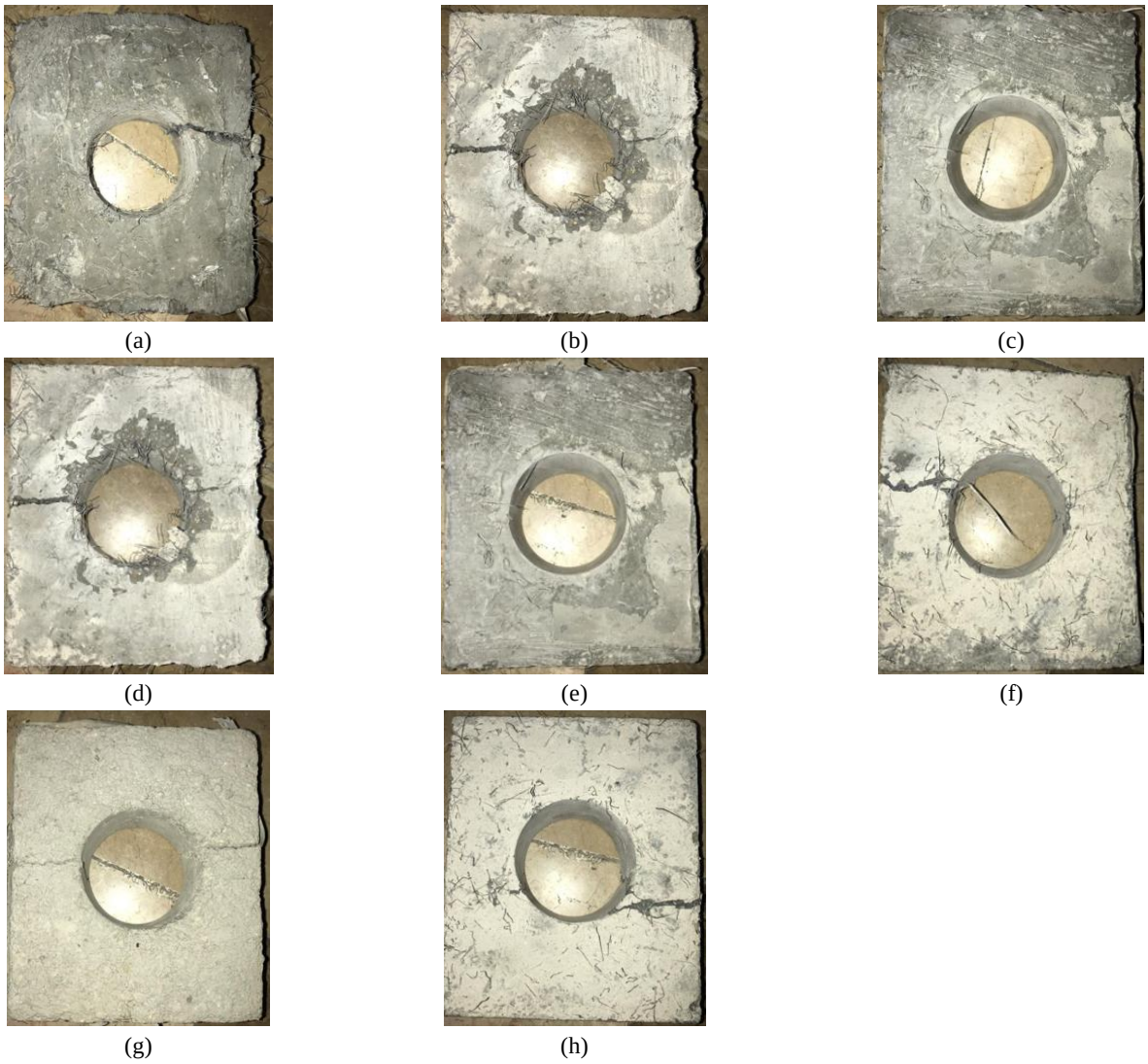

Fig. 9 The direct tensile failure pattern in UHPC specimens

3.1.2 Specimen test method

The complete setup of a CTLC device is illustrated in Figs. 7(a)-(c). These figures show the useful procedure for performing the direct tensile strength measurement process for the concrete samples in the laboratory. Three views of direct tensile fracturing in a typical concrete specimen (fitted in CTLC device can be visualized in Figs. 7(a)-(c). This setup is managed in such a manner that the upper section of the specimen is in contact with the lower cylindrical steel while at the same time, the lower section is in contact with the upper cylindrical steel and then the setup is completed. This completed setup is placed in the conventional uniaxial compression loading frame in the laboratory. By this procedure, during the loading process, the upper part of the specimen is compressing its lower part while moving down and at the same time the lower part of the specimen is compressing downward (Fig. 7) so that a direct tensile loading is applied to the specimen.

3.2 UHPC specimen's preparation for CTLC device

The direct tensile strength of the UHPC with a specific gravity of 2.75 g/cm^3 is measured in the laboratory using some specially prepared UHPC specimens for CTLC device. The UHPC beam specimen size is 150 × 60 × 190 mm high with a central hole of 75 mm diameter. In this study, the ratio of central hole diameter to that of the sample's width is taken as 0.5.

3.3 Direct tensile strength test by CTLC

In this study, a Universal Tensile Testing device (UTTM) is used as shown in Fig. 8. The CTLC device together with the UHPC specimens already prepared in the laboratory can be used to complete the required arrangement for measuring the direct tensile strength of the concrete in UTTM (Fig. 8). In this experimental approach, the UTTM have a conventional uniaxial compression frame which can provide the required uniaxial compression for the CTLC device already contained a UHPC specimen. The loading frame of UTTM is specially designed for applying a uniaxial compressive load to the end plates of the CTLC device via a 5-tons gearbox load cell which can electronically record the applied load increments during

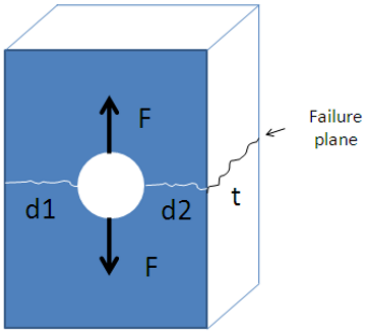

Fig. 10 Failure plane in direct tensile test

Table 7 Direct tensile strengths of UHPC specimens

Experimental direct tensile strength (MPa)			
10.5	10.3	10.4	10.5
10.4	10.35	10.6	10.6
10.6	10.5	10.6	10.3
10.5	10.6	10.3	
Average			
10.47			

tensile testing process. During the testing operation, a constant loading rate of 0.02 MPa/s is applied to minimize its effects on the final testing results of the direct tensile strength of UHPC. This loading rate is suggested for the tensile strength measurement using a rock splitting approach, ASTM D3967-16 (2008). UTTM is powered by a single-phase electricity applying through a rigid frame of 5 tons loading capacity and can be effectively used for measuring the direct and indirect tensile strengths, the uniaxial compressive and the fracture toughness of concrete, rocks, ceramics, mortars and asphalts. However, UTTM cannot be used for measuring the uniaxial strength of relatively hard rocks but it can be used for measuring the compressive strength of rock like materials, soft and medium rocks, ceramics and asphalts, successfully.

In the present research, the UTTM with CTLC device is used to measure the direct tensile strength of UHPC specimens. Therefore, 15 pre-holed rectangular specimens of UHPC are prepared and placed in the CTLC device for testing with UTTM in a rock mechanics laboratory. Figs. 9(a)-(h) show the failure and crack propagation process in 8 failed specimens. These figures show that when the UHPC specimens are subjected to tensile loading the horizontal line cracks are getting started from the boundary of the center holes and extend through the specimens' width.

3.4 Laboratory measurement of the direct tensile strengths of UHPC specimens

In the direct tensile strength measuring approach explained in this study, the distribution of induced tensile stress at the UHPC specimen is more than that of the far field tensile stress. Therefore, the far field tensile stress cannot be directly considered as the real tensile strength of the concrete specimen. However, the following simple formula is suggested to be used for the calculation of the direct tensile strength (σ_t) of the UHPC specimens

$$\sigma_t = \frac{F}{(d1 + d2) \times t} \tag{6}$$

In this equation, σ_t is the tensile strength of the material in kg/cm^2, F is the applied force in kg, t is thickness of the specimen (in cm) and, $d1$ and $d2$ (expressed in cm) are the specimen's width on either side of the central hole (Fig. 10). It is to be note that Sarfarazi *et al.* (2016) rendered a new criteria for measuring a tensile strength of concrete based on stress concentration around the internal hole.

However, the average direct tensile strength of UHPC specimens obtained by using CTLC device implemented in UTTM is about 10.47 MPa. The details of these experimental results are given in Table 7.

Further verification of the direct tensile strength obtained by using the CTLC device in UTTM can be made by simulating the concrete testing specimens through some numerical techniques such as the Discrete Element Method (DEM) and extended finite element method (XFEM). In the present work, the Particle Flow Code in Two-Dimensions (PFC2D) based on DEM and the ABAQUS software based on XFEM are both used to verify the experimental direct tensile strength values for UHPC.

4. Numerical simulation of the UHPC specimens used in tensile strength tests (particle flow code)

In this study, The CTLC device using specially made rectangular specimens with a central hole is implemented in UTTM to directly measure the tensile strength of UHPC specimens in a rock mechanics laboratory. In this section, it is tried to verify this new approach by the most sophisticated numerical methods i.e., the DEM and XFEM.

4.1 Simulating the UHPC specimens by DEM

The UHPC specimens used for CTLC device are numerically simulated using a sophisticated particle flow code for PFC2D analysis of geo-mechanical problems based on DEM. In this code, each specimen is considered as an assembly of circular discs which are bonded to the neighboring discs at the contact points by the contact forces. The whole particle assembly is confined by the planar side walls to complete the specimens simulating process. Therefore, in this simulating procedure, the UHPC specimens are modelled in form of material particles bonded to each other at the contact points with their neighboring particles. The internal contact forces keeping all the particles to be in contact with each other in the whole particle assembly. In the discrete analysis of geo-materials (such as rock and concrete), two types of bonding models i.e., the contact and parallel are basically used. In the contact bonded model, a very thin layer of matrix bonding each two neighboring particles is used to simulate the

Table 8 Micro properties used to numerically simulate the intact UHPC specimens

Parameter	Value	Parameter	Value
Type of particle	disc	Stiffness ratio	2
Density (kg/m3)	3600	Particle friction coefficient	0.5
Minimum radius (mm)	0.27	Contact bond normal strength, mean (MPa)	75
Size ratio	1.56	Contact bond normal strength, SD (MPa)	2
Porosity ratio	0.08	Contact bond shear strength, mean (MPa)	75
Damping coefficient	0.7	Contact bond shear strength, SD (MPa)	2
Contact young modulus (GPa)	55	Thickness of disc (mm)	1

(a)

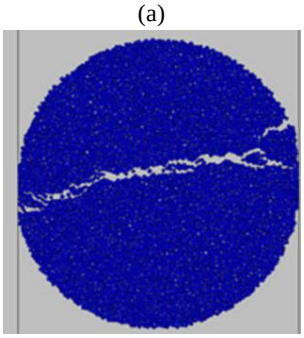

(b)

Fig. 11 (a) Experimental Brazilian tensile strength test; (b) numerically simulated Brazilian tensile strength test

physical behavior of the material. In the parallel bonded model, there is a radius of bonding (for each bond) at the contact point between each two neighboring particles. Therefore, a parallel bonded model with zero bonding radius at the contact points is a contact bonded model for which there is no normal and/or shear stiffness and there is no bending moment at the contact points where only contact forces are acting. The contact bonded and parallel bonded models are very close to each other so that a contact bonded model is the same as a parallel bonded model but with zero bonding radius. However, in a contact bonded model the shear and tensile strengths should be assigned to allow for the geo-material to be able to resist against the applied tensile and shear forces under various loading conditions in the surface and underground structures (Itasca Consulting Group Inc. 2003, Potyondy and Cundall 2004). In PFC2D some special algorithms are established by Cundall and Strack (1979) which generate both the contact and parallel bonded models for any particular particle assembly. They explained the relations between the macro-mechanical parameters measured in the laboratory with the micro-mechanical properties required in the numerically simulated models. Some of the most important geo-mechanical properties include: The contact modulus, the coefficient of friction and the stiffness ratio Kn/Ks of the particles and their bonding within the particle assembly representing the geo-material specimen. The limitations of DEM is Donze *et al*. (2009): (a) Fracture is closely related to the size of elements, and that is so-called size effect; (b) Cross effect exists because of the difference between the size and shape of elements with real grains; (c) In order to establish the relationship between the local and macroscopic constitutive laws, data obtained from classical geomechanical tests which may be impractical are used.

4.1.1 Numerical simulation of splitting or Brazilian tensile strength test

For an accurate simulating of UHPC specimens by PFC2D, a standard calibration technic is used by simulating the Brazilian tensile testing of rock samples with this software. Potyondy and Cundall (2004) suggested a standard calibrating procedure for PFC2D by adopting the micro-properties of a typical geo-material model given in Table 8. They used 5615 particles to model a Brazilian disc specimen of 54 mm in dia. They assumed a constant loading speed of 0.016 m/s to move the lateral walls of this specimen toward each other so that a quasi-static equilibrium state can be established for the geo-material (rock or concrete) specimens. They fixed a porosity of 0.08 for the calibrating model which may be different for the actual rock sample.

Fig. 11(a) shows the Brazilian discs used for measuring the tensile strength of the concrete while Fig. 11(b) shows the numerically simulated one modeled by PFC2D. The numerical and experimental values of the indirect tensile strength values for the concrete specimens are 10.90 and 10.75 MPa, respectively. Therefore, these results are very close to each other and it is concluded that the calibrated micro-parameters can be used for modeling the UHPC specimens for estimating their direct tensile testing using the CTLC device.

4.1.2 Numerical simulation of CTLC testing specimens using particle flow code (PFC)

Fig. 12 shows a box model of a UHPC specimens with the dimensions of 75 mm × 100 mm which is simulated by PFC2D. A total number of 11,179 circular discs with a minimum radius of 0.27 mm are used to build the particle assembly representing the modeled specimen. Figs. 12(a)-

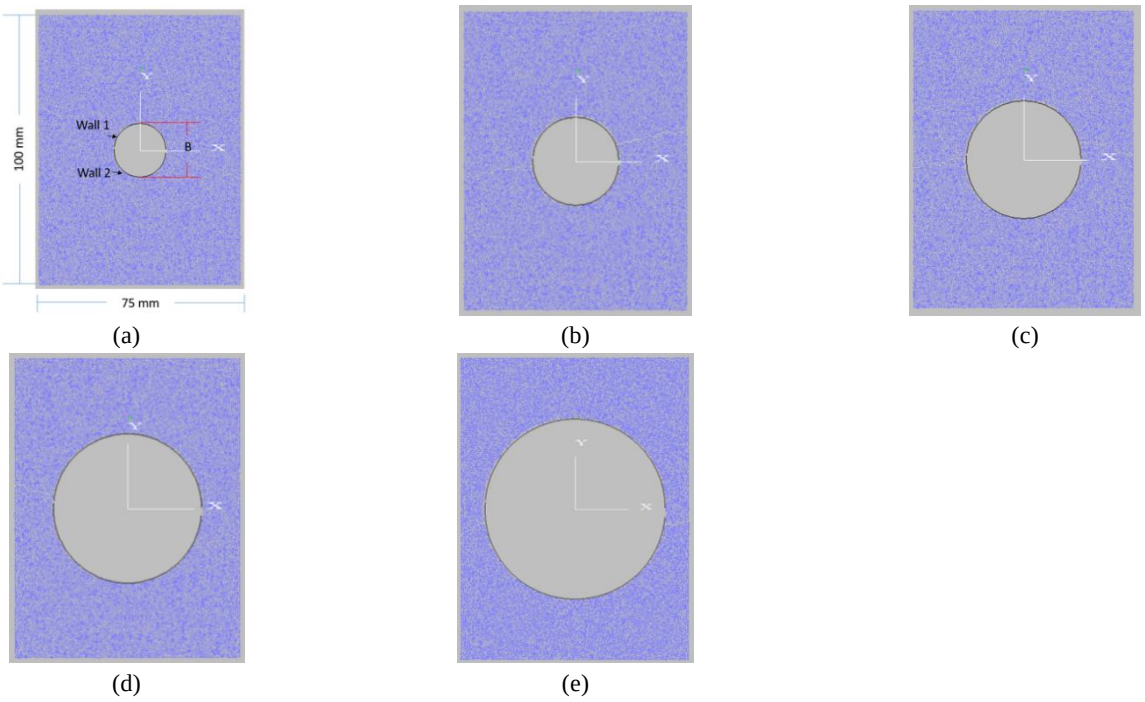

Fig. 12 Specification for the numerical modelling of CTLT testing specimens with a hole diameter of (a) 10 mm; (b) 15 mm; (c) 20 mm; (d) 25 mm; (e) 30 mm

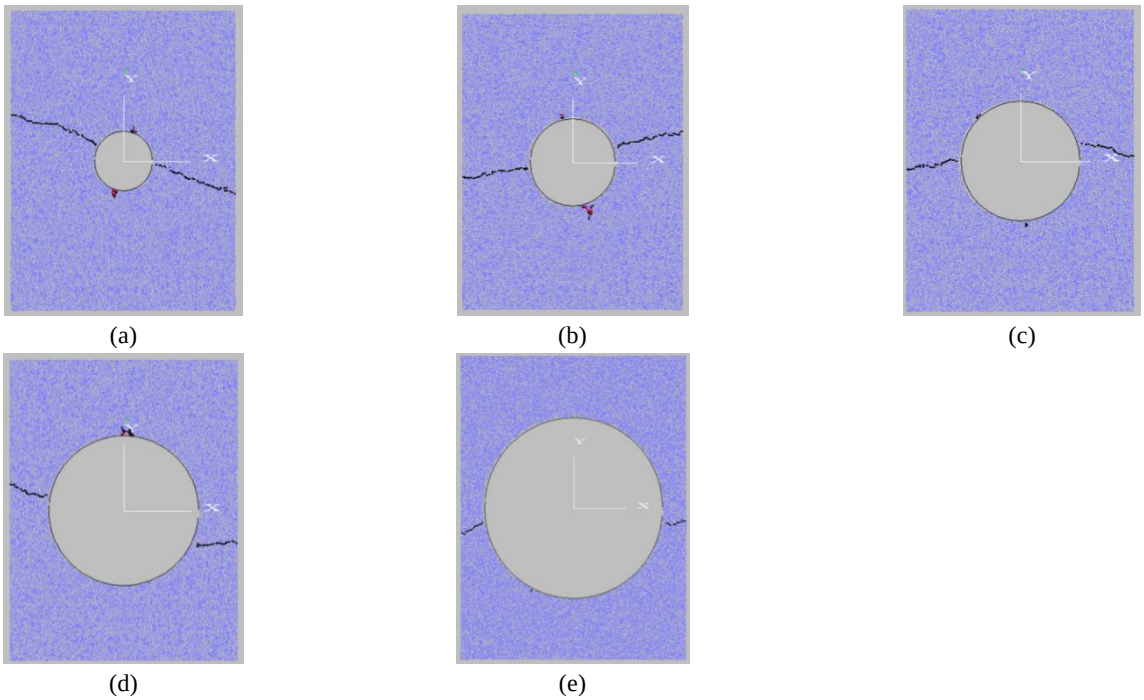

Fig. 13 Failure pattern of the numerically modeled CTLT specimens each containing a central hole of diameter (a) 10 mm; (b) 15 mm; (c) 20 mm; (d) 25 mm; (e) 30 mm

(e) show the simulated box models each having a hole of various diameters, *B* (*B* = 10, 15, 25 and 30 mm). This hole is at the central part of the box model which represents the rectangular CTLC type specimens as used in UTTM to measure the direct tensile strength of UHPC. After preparing the numerical model, two semi-circular load- in contact with the central hole (Fig. 12(a)).

4.3 Tensile strength and crack propagation process in PFC2D simulated CTLC specimens

The process of CTLC specimens' failure and their fracturing pattern are illustrated in Figs. 13(a)-(e). The crack propagation process of these specimens during the testing operation is also shown. The tensile (primary) cracks

Table 9 The numerical values of direct tensile strength estimated by PFC2D

The internal hole diameter (mm)	Numerical direct tensile strength (MPa)
10	10.8
15	10.6
20	10.78
25	10.7
30	10.65

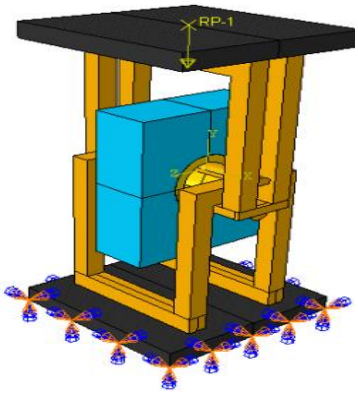

Fig. 14 The schematic view of compressive to tensile load convertor device

are shown by black lines while the red lines demonstrate the shear or secondary cracks produced during the failure process of the modelled specimens. As a whole it is concluded that during the failure process of each CTLC specimen two horizontal line cracks are produced and extended through the center of the specimen's hole on the either side of the modelled UHPC specimens. Comparing these numerically gained results with those already shown in Fig. 9 for the experimental tests the same scenario can be visualized which validates the experimental testing procedure suggested in this research for the direct tensile testing measurement of UHPC.

Table 9 gives the numerical values of the direct tensile strengths obtained by PFC2D. Comparing these results with those obtained experimentally in Table 7. One can easily visualize that these two set of direct tensile strength values are very close to each other which again the validity of both experimental and numerical procedures adopted in this study is approved. Also, by comparison between direct tensile strength estimated by PFC2D (10.7 MPa) and numerical Brazilian tensile strength (10.9 MPa), it can be concluded that the tensile strength predicted by Brazilian test was more than that by direct tensile test. It was due to stress gradient on the failure surface in Brazilian test

4.4 Simulating CTLC specimens using ABAQUS software

In this section the tensile stress distribution in rectangular model containing a central hole used in CTLC device is simulated by ABAQUS software (Fig. 14).

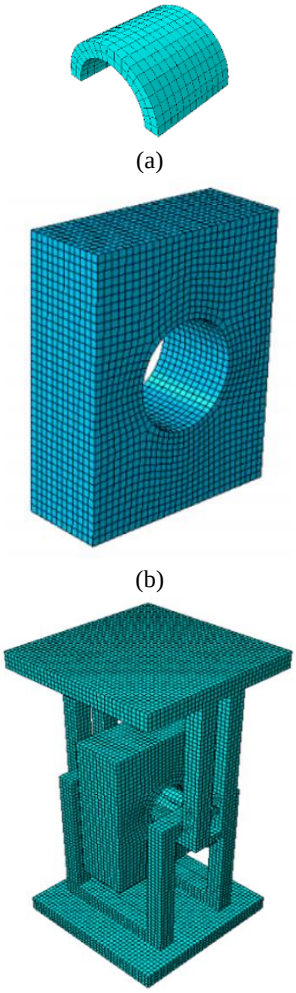

(a)

(b)

(c)

Fig. 15 ABAQUS software used to simulate (a) semi cylinder; (b) specimen model and (c) CTLC device

Figs. 15(a)-(c) show the numerical simulation of a CTLC device containing a rectangular specimen with a central hole.

It may be assured that the CTLC specimen simulation by ABAQUS may not have a significant residual compressive stress at the mid length of the specimen. However, the proposed method in this study assures that the total specimen failure is due to pure tensile loading more beyond that of the shear stresses to get a chance to be produced at both ends of the specimen. It is also assured that the tensile failure occurs at the mid-lengths of the specimen on either side of the central hole due to pure tensile loading. The tensile stress distribution in the CTLC specimen as predicted by XFEM (ABAQUS software) is shown in Fig. 16. As shown in this figure, the tensile stress concentration zones are at the left and right sides of the central hole where the tensile cracks can be produced to cause the specimen's failure.

It is also quite evident that the compressive stresses are also concentrated at the top and bottom of the central hole.

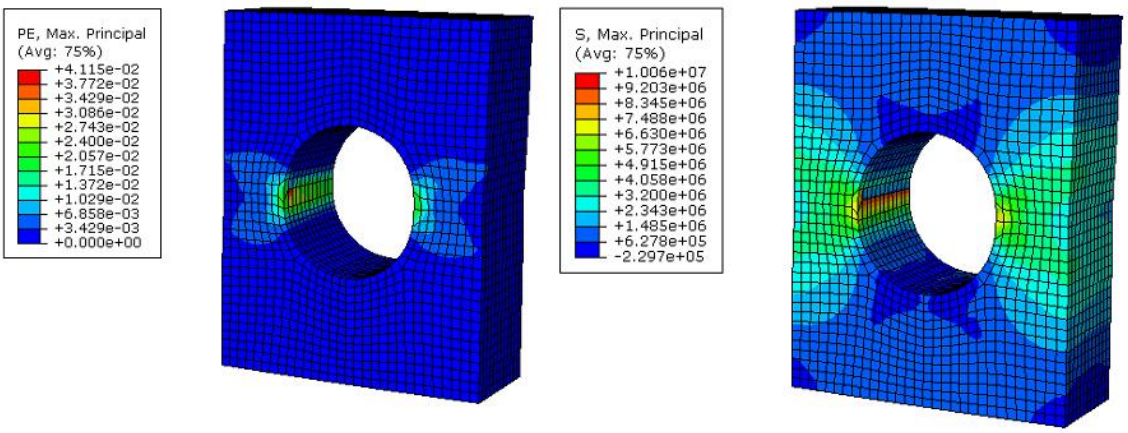

Fig. 16 Tensile stress distribution in the model

As the tensile strengths of geo-materials are less than their compressive strengths one may expect that in all these models the failure zone is situated in the left and right sides of the central hole much more before that the failure can be started under the compression at the vertical-section of the CTLC specimen. Therefore, it can be concluded that the proposed technique is suitable for determination of direct tensile strength of concrete, rocks, rock like materials and composite.

5. Conclusions

In this study, the experimental tests for the direct tensile strength measurement of UHPC were numerically modeled by using the discrete element method and FEM. The results show that:

• A specially developed CTLC device containing a rectangular specimen with a central hole was designed to be able to measure the direct tensile strength of ultra-high performance concrete

• The measured direct tensile strength of UHPC specimens can be calculated by a new simple equation proposed in this study and was about 10.47 MPa.

• It has been concluded that the specimen failure occurs due to pure tensile stresses at both left and right sides of the CTLC specimen's central hole.

• PFC2D simulations of the direct tensile strength measuring specimen and ABAQUS simulation of the tested CTLC specimens both demonstrate the validity and capability of the proposed testing procedure for the direct tensile strength measurement of UHPC specimens.

References

Abrishambaf, A., Barros, J.A. and Cunha, V.M. (2015), "Tensile stress-crack width law for steel fibre reinforced self-compacting concrete obtained from indirect (splitting) tensile tests", *Cement Concrete Compos*., **57**, 153-165. https://doi.org/10.1016/j.cemconcomp.2014.12.010.

Akbas, S. (2016), "Analytical solutions for static bending of edge cracked micro beams", *Struct. Eng. Mech., Int. J.*, **59**(3), 579-599. https://doi.org/10.12989/sem.2016.59.3.579.

Alhussainy, F., Hasan, H.A., Rogic, S., Sheikh, M.N. and Hadi, M.N. (2016), "Direct tensile testing of self-compacting concrete", *Constr. Build. Mater*., **112**, 903-906. https://doi.org/10.1016/j.conbuildmat.2016.02.215.

Aliabadian, Z., Zhao, G.F. and Russell, A.R. (2019), "Failure, crack initiation and the tensile strength of transversely isotropic rock using the Brazilian test", *Int. J. Rock Mech. Min. Sci*., **122**, 104073. https://doi.org/10.1016/j.ijrmms.2019.104073.

ASTM D2936-08 (2008), *Standard Test Method for Direct Tensile Strength of Intact Rock Core Specimens*, Annual Book of ASTM Standards, ASTM, West Conshohocken, USA.

ASTM D2938-86 (1986), Test Method for Unconfined Compressive Resistance of Intact Rock Core Specimens, ASTM Designation, USA.

ASTM D3967-16 (2008), *Standard Test Method for Splitting Tensile Strength of Intact Rock Core Specimens*, Annual Book of ASTM Standards, ASTM, West Conshohocken, USA.

Bi, J., Zhou, X.P. and Qian, Q. (2016), "The 3D numerical simulation for the propagation process of multiple pre-existing flaws in rock-like materials subjected to biaxial compressive loads", *Rock Mech. Rock Eng*., **49**(5), 1611-1627. https://doi.org/10.1007/s00603-015-0867-y.

Bieniawski, Z.T. and Hawkes, I. (1978), "Suggested method for determining tensile strength of rock materials", *Int. J. Rock Mech. Min. Sci. Geomech*., **1**, 99-103.

CEB-FIB (2010), The Fib Model Code for Concrete Structures Case Postale 88, CH-1015 Lausanne, Switzerland.

Chen, W.F. and Trumbauer, B.E. (1972), "Double-punch test and tensile strength of concrete", *J. Mater*., **7**(2) 148-154.

Cundall, P.A. and Strack, O.D.L. (1979), "A discrete numerical model for granular assemblies", *Geotechnique*, **29**(1), 47-65. https://doi.org/10.1680/geot.1979.29.1.47.

Donze, F.V., Richefeu, V. and Magnier, S.A. (2009), "Advances in discrete element method applied to soil rock and concrete mechanics", *Elec. J. Geol. Eng*., **8**, 1-44.

Erarslan, N. and Williams, D.J. (2012), "Experimental, numerical and analytical studies on tensile strength of rocks", *Int. J. Rock Mech. Min. Sci*., **49**, 21-30. https://doi.org/10.1016/j.ijrmms.2011.11.007.

Ghaffar, A., Chaudhry, M.A. and Kamran Ali, M. (2005), "A new approach for measurement of tensile strength of concrete", *J. Res. Sci*., **16**(1), 1-9.

Hibbitt, H.D., Karlsson, B.I. and Sorensen, E.P. (2012), ABAQUS User's Manual, Dassault Systèmes Simulia Corp., USA.

Hillerborg, A. (1989), The Compression Stress-Strain Curve for Design of Reinforced Concrete Beams, Fracture Mechanics: Application to Concrete, ACI-SP-118, Detroit, USA.

Hordijk, D.A. (1992), "Tensile and tensile fatigue behaviour of

concrete experiments, modelling and analyses", *Heron*, **37**(1), 3-79.
Itasca Consulting Group Inc. (2003), "PFC2D (particle flow code in 2dimensions) version 3.0", *ICGI*, **41**(8), 1329-1364.
Khan, M.I. (2012), "Direct tensile strength measurement of concrete", *Appl. Mech. Mater.*, **117**, 9-14. https://doi.org/10.4028/www.scientific.net/AMM.117-119.9.
Kim, J. and Taha, M.R. (2014), "Experimental and numerical evaluation of direct tension test for cylindrical concrete specimens", *Adv. Civ. Eng.*, **2014**, 156926. https://doi.org/10.1155/2014/156926.
Li, S., Wang, H., Li, Y., Li, Q., Zhang, B. and Zhu, H. (2016), "A new mini-grating absolute displacement measuring system for static and dynamic geomechanical model tests", *Measurement*, **82**, 421-431. https://doi.org/10.1016/j.measurement.2017.04.002.
Liao, Z.Y., Zhu, J.B. and Tang, C.A. (2019), "Numerical investigation of rock tensile strength determined by direct tension, Brazilian and three-point bending tests", *Int. J. Rock Mech. Min. Sci.*, **115**, 21-32. https://doi.org/10.1016/j.ijrmms.2019.01.007.
Liu, Y., Dai, F., Xu, N., Zhao, T. and Feng, P. (2018), "Experimental and numerical investigation on the tensile fatigue properties of rocks using the cyclic flattened Brazilian disc method", *Soil Dyn. Earthq. Eng.*, **105**, 68-82. https://doi.org/10.1016/j.soildyn.2017.11.025.
Martin, C.D. (2014), "The direct and Brazilian tensile strength of rock in the light of size effect and bimodularity", *Proceedings of the American Rock Mechanics Association: 48th U.S. Rock Mechanics/Geomechanics Symposium*, Minneapolis, M.N., USA.
Mier, V.J. (1986), "Multiaxial strain-softening of concrete", *Mater. Struct.*, **19**(111), 179-200. https://doi.org/10.1007/BF02472035.
Mohammad, A. (2016), "Statistical flexural toughness modeling of ultra-high-performance concrete using response surface method", *Comput. Concrete, Int. J.*, **17**(4), 477-488. https://doi.org/10.12989/cac.2016.17.4.477.
Omar, H., Ahmad, J., Nahazanan, H., Mohammed, T.A. and Yusoff, Z.M. (2018), "Measurement and simulation of diametrical and axial indirect tensile tests for weak rocks", *Measurement*, **127**, 299-307. https://doi.org/10.1016/j.measurement.2018.05.067.
Pan, B., Gao, Y. and Zhong, Y. (2014), "Theoretical analysis of overlay resisting crack propagation in old cement concrete pavement", *Struct. Eng. Mech., Int. J.*, **52**(4), 167-181. https://doi.org/10.12989/sem.2014.52.4.829.
Potyondy, D.O. and Cundall, P.A. (2004), "A bonded-particle model for rock", *Int. J. Rock Mech. Min. Sci.*, **41**(8), 1329-1364. https://doi.org/10.1016/j.ijrmms.2004.09.011.
Ramadoss, P. (2014), "Combined effect of silica fume and steel fibers on the splitting tensile strength of high-strength concrete", *Int. J. Civ. Eng.*, **12**(1), 99-103.
Ramadoss, P. and Nagamani, K. (2006), "Investigations on the tensile strength of high-performance fiber reinforced concrete using statistical methods", *Comput. Concrete, Int. J.*, **3**(6), 389-400. https://doi.org/10.12989/cac.2006.3.6.389.
Ramadoss, P. and Nagamani, K. (2008), "Tensile strength and durability characteristics of high-performance fiber reinforced concrete", *Arab. J. Sci. Eng.*, **33**(2), 307-319.
Ramadoss, P. and Nagamani, K. (2013), "Stress-strain behavior and toughness of high-performance steel fiber reinforced concrete in compression", *Comput. Concrete., Int. J.*, **11**(2), 149-167. https://doi.org/10.12989/cac.2013.11.2.149.
Sardemir, M. (2016), "Empirical modeling of flexural and splitting tensile strengths of concrete containing fly ash by GEP", *Comput. Concrete, Int. J.*, **17**(4), 489-498. https://doi.org/10.12989/cac.2016.17.4.489.
Sarfarazi, V., Ghazvinian, A., Schubert, W., Nejati, H. and Hadei, R. (2016), "A new approach for measurement of tensile strength of concrete", *Periodica Polytech. Civ. Eng.*, **60**(2), 199-203. https://doi.org/10.3311/PPci.8328.
Sarfarazi, V., Haeri, H. and Bagher Shemirani, A. (2017), "Direct and indirect methods for determination of mode I fracture toughness using PFC2D", *Comput. Concrete, Int. J.*, **20**(1), 39-47. https://doi.org/10.12989/cac.2017.20.1.039.
Shang, J., Duan, K., Gui, Y., Handley, K. and Zhao, Z. (2018), "Numerical investigation of the direct tensile behaviour of laminated and transversely isotropic rocks containing incipient bedding planes with different strengths", *Comput. Geotech.*, **104**, 373-388. https://doi.org/10.1016/j.compgeo.2017.11.007.
Shaowei, H., Aiqing, X., Xin, H. and Yangyang, Y. (2016), "Study on fracture characteristics of reinforced concrete wedge splitting tests", *Comput. Concrete, Int. J.*, **18**(3), 337-354. https://doi.org/10.12989/cac.2016.18.3.337.
Shuraim, A.B., Aslam, F., Hussain, R. and Alhozaimy, A. (2016), "Analysis of punching shear in high strength RC panels-experiments, comparison with codes and FEM results", *Comput. Concrete, Int. J.*, **17**(6), 739-760. https://doi.org/10.12989/cac.2016.17.6.739.
Silva, R.V., De Brito, J. and Dhir, R.K. (2015), "Tensile strength behaviour of recycled aggregate concrete", *Constr. Build. Mater.*, **83**, 108-118. https://doi.org/10.1016/j.conbuildmat.2015.03.034.
Swaddiwudhipong, S., Lu, H.R. and Wee, T.H. (2003), "Direct tension test and tensile strain capacity of concrete at early age", *Cem. Concrete Res.*, **33**, 2077-2084. https://doi.org/10.1016/S0008-8846(03)00231-X.
Tran, K.Q., Satomi, T. and Takahashi, H. (2019), "Tensile behaviors of natural fiber and cement reinforced soil subjected to direct tensile test", *J. Build. Eng.*, **24**, 100748. https://doi.org/10.1016/j.jobe.2019.100748.
Van Mier, J.G.M. (1992), "Assesment of strain softening curves for concrete", *TU Delft*, Mekelweg, Netherlands.
Vonk, R.A. (1993), "A micromechanical investigation of softening of concrete loaded in compression", *Heron*, **38**(3), 3-94.
Wang, Q., Jias, X., Kou, S., Zang, Z. and Lindqvist, P.A. (2004), "The flattened Brazilian disc specimen used for testing elastic modulus, tensile strength and fracture toughness of brittle rocks: Analytical and numerical results", *Int. J. Rock Mech. Min. Sci.*, **41**, 245-253. https://doi.org/10.1016/S1365-1609(03)00093-5.
Wei, X.X. and Chau, K.T. (2013), "Three dimensional analytical solution for finite circular cylinders subjected to indirect tensile test", *Int. J. Solids Struct.*, **50**, 2395-2406. https://doi.org/10.1016/j.ijsolstr.2013.03.026.
Xie, N.X. and Liu, W.Y. (1989), "Determining tensile properties of mass concrete by direct tensile test", *ACI Mater. J.*, **86**(3) 214-219.
Yaylac, M. (2016), "The investigation crack problem through numerical analysis", *Struct. Eng. Mech., Int. J.*, **57**(6), 1143-1156. https://doi.org/10.12989/sem.2016.57.6.1143.
Zain, M.F.M., Mahmud, H.B., Ilham, A. and Faizal, M. (2002), "Splitting tensile strength of high-performance concrete", *Cem. Concrete. Res.*, **32**, 1251-1257.
Zhang, Z.X. (2002), "An empirical relation between mode I fracture toughness and the tensile strength of rock", *Int. J. Rock Mech. Min. Sci. Geomech.*, **93**, 401-406.
Zhang, D., Hou, S., Bian, J. and He, L. (2016), "Investigation of the micro-cracking behavior of asphalt mixtures in the indirect tensile test", *Eng. Fract. Mech.*, **163**, 416-425. https://doi.org/10.1016/j.engfracmech.2016.05.020.
Zheng, W., Kwan, A.K.H. and Lee, P.K.K. (2001), "Direct tension test of concrete", *ACI Mater. J.*, **98**(1) 63-71.
Zhou, F.P. (1988), "Some aspects of tensile fracture behaviour and structural response of cementitious materials", Report TVBM-1008, Lund Institute of Technology, Lund, Sweden.

Zhou, X.P. and Yang, H.Q. (2012), "Multiscale numerical modeling of propagation and coalescence of multiple cracks in rock masses", *Int. J. Rock Mech. Min. Sci*., **55**, 15-27. https://doi.org/10.1016/j.ijrmms.2012.06.001.

Zhou, X.P. and Wang, Y. (2016), "Numerical simulation of crack propagation and coalescence in pre-cracked rock-like Brazilian disks using the non-ordinary state-based peridynamics", *Int. J. Rock Mech. Min. Sci*., **89**, 235-249. https://doi.org/10.1016/j.ijrmms.2016.09.010.

Zhou, X.P., Zhang, Y.X., Ha, Q.L. and Zhu, K.S. (2008), "Micromechanical modelling of the complete stress–strain relationship for crack weakened rock subjected to compressive loading", *Rock Mech. Rock Eng*., **41**(5), 747-769. https://doi.org/10.1007/s00603-007-0130-2.

Zhou, X.P., Bi, J. and Qian, Q. (2015), "Numerical simulation of crack growth and coalescence in rock-like materials containing multiple pre-existing flaws", *Rock Mech. Rock Eng.*, **48**(3), 1097-1114. https://doi.org/10.1007/s00603-014-0627-4.

CC